Wide-Range Robust Control of Combustion Instability

Boe-Shong Hong, Vigor Yang and Asok Ray
Mechanical Engineering Department
The Pennsylvania State University
University Park, Pennsylvania 16802, USA

Abstract

This paper presents the concept and design of a two-layer robust control system for suppression of combustion instabilities over a wide range of operation. The control law synthesis based on a multiple-time-scale model of combustion dynamics. Control actions on the fast-time scale are provided by secondary fuel injection, realized as modulation of the primary fuel flow, and are gain-scheduled according to the variations of mean-flow temperature and velocity on the slow-time scale. A linear parameter varying (LPV) L_2-gain control law is formulated in the setting of differential game theory. Simulation experiments have been conducted to evaluate the control law under wide-range operation of a generic combustor in terms of the trade-off among: (i) fuel injection rate and pressure oscillation; (ii) transient and steady responses; and (iii) stability robustness and performance.

1. Introduction

Unsteady motions in confined combustion chambers often result from mean-flow dependent interactions between heat release and acoustic oscillations. The underlying physical mechanisms involve a wide range of time scales that can be broadly classified into two categories: one representing mean-flow motions on a slow time-scale and the other representing acoustic oscillations on a fast time-scale. The disparity of time scales allows for the development of a hierarchically structured control law for regulating the various processes involved. The overall combustor system may consist of two interacting modules: slow-time supervisory controller and fast-time flame controller, as illustrated in Fig.1 [1]. The slow-time supervisory controller in the outer loop attempts to optimize the overall combustor performance and pollutant emissions based on the measurements of quasi-steady variables, and to identify the flame control parameters that determine the operating points of the fast dynamic phenomena such as pressure oscillations. The flame controller in the inner loop is responsible for suppression of combustion instability and for prevention of lean blowout of the flame. When coupled with a global engine control system, such a two-layer strategy will lead to an energy-efficient and clean system for propulsion and power-generation applications.

As part of their research on feedback control of combustion instabilities in various propulsion systems, Yang and co-workers established a series of control designs with distributed actuation [2-6]. The recent work by Hong et al. [6] was based on the H_∞-optimization, which guaranteed robust stability and performance within specified bounds of model and parameter uncertainties as well as sensor noise and plant disturbance. The nominal system parameters, however, were treated as time-invariant constants, thereby rendering the control laws valid only for narrow range of operating conditions. The present paper attempts to remedy this deficiency by taking into account the temporal variations of mean-flow dynamics in such a unified manner that the resultant control laws function effectively over a wide-range of operations. The work incorporates an H_∞-based linear-parameter-varying (LPV) control [7,8] for modulating combustion dynamics. Its major contributions beyond the previous studies on narrow-range control [6] are

- establishment of a two-time-scale model of combustion dynamics for robust control systems analysis and synthesis, and
- development of an observer-embedded robust LPV control law within the aforementioned two-layer architecture.

The paper is organized in six sections including the introduction. Section 2 develops a two-time-scale model of combustion dynamics in a liquid-fueled propulsion system. The wide-range robust control law is formulated and analyzed in Sections 3 and 4, respectively, based on the concept of differential game theory. Section 5 presents the results of simulation experiments for evaluating the system performance under different control laws. The paper is summarized and concluded in Section 6 with recommendations for future research.

2. A Two-Time-Scale Model of Combustion Dynamics

The disparate time scales involved in the various combustion and flow processes allows for the decomposition of the conservation laws into two settings governing slow-time mean-flow dynamics and fast-time acoustic dynamics, respectively. The fast-time dynamics is parametrically dependent on the slow-time mean-flow variables. Using a spatial-averaging procedure equivalent to modal analysis, a family of linear finite-dimensional parameterized models is derived for parameter-dependent robust feedback control design.

The equations governing the dynamics of a liquid-fueled combustion device with feedback control actuators can be succinctly expressed as [2]:

$$\frac{\partial \rho}{\partial t} + \mathbf{v}_g \cdot \nabla \rho + \rho \nabla \cdot \mathbf{v}_g = W + W_c \tag{1}$$

$$\rho \frac{\partial \mathbf{v}_g}{\partial t} + \rho \mathbf{v}_g \cdot \nabla \mathbf{v}_g + \nabla p = F + F_c \tag{2}$$

$$\frac{\partial p}{\partial t} + \bar{\gamma} p \nabla \cdot \mathbf{v}_g + \mathbf{v}_g \cdot \nabla p = P + P_c \tag{3}$$

where the source terms W, F, and P represent the two-phase interactions and combustion influence, and W_c, F_c and P_c the total mass, momentum and energy control inputs, respectively.

It is apparent from experimental or computational observation that motions in the fluid field take place in two time-

Paper presented at the RTO AVT Symposium on "Active Control Technology for Enhanced Performance Operational Capabilities of Military Aircraft, Land Vehicles and Sea Vehicles", held in Braunschweig, Germany, 8-11 May 2000, and published in RTO MP-051.

scales: one representing the mean-flow motion with a slower time-scale and larger amplitude-order, and the other representing acoustic motion with fast time-scale and smaller amplitude-order. Now, the purpose is to decompose each single conservation law, described in Eqs. (1), (2) and (3), into two time scales describing the slow behavior of mean-flow motions and primary combustion inputs, and fast behavior of acoustic oscillations and secondary-fuel injection into the combustion chamber. The components of the fluid-variable vector $x \equiv [\rho \quad \mathbf{v}_g \quad p]^T$ in the following table have their own time-scales and amplitude-orders where the subscripts s and f represent the slow and fast time scales, respectively.

Table I Two Time-scaled Motions

	Time scales	Amplitude Orders
Mean-flow motion $\tilde{x}(t_s)$	$t_s = \varepsilon_s t$	$A_s \approx \varepsilon_s A_t$
Acoustic motion $x'(t_f)$	$t_f = \varepsilon_f t$	$A_f \approx \varepsilon_f A_t$

In the table, the referenced time-scale and amplitude-order are denoted as t and A_t, respectively, and the referenced time t here is taken as the regular time used in the physical laws. The time-scale and amplitude order are described by the pair $(\varepsilon_s, \varepsilon_f)$, with $\varepsilon_f \sim o^1(\varepsilon_s)$ where $\left|\frac{o^1(\theta)}{\theta}\right| \to 0 \; as \; \theta \to 0$.

Remark 1: When observing events in the fast-time scale, $t_f \sim t$ implying that $\varepsilon_f \sim 1$ and $\varepsilon_s \gg 1$. Similarly, when observing events in the slow-time scale, $t_s \sim t$ implying that $\varepsilon_s \sim 1$ and $\varepsilon_f \ll 1$.

The combustion control inputs (W_c, F_c, P_c) are also decomposed as two components: one is the primary component with the same (i.e., slow) time-scale and amplitude-order as those of the mean-flow motions, and the other is secondary component with the same (i.e., fast) time-scale and amplitude-order as those of acoustic oscillations. The former primarily affects the mean-flow field, while the latter is a modulated component influencing the acoustic field. Similar treatments are applied to the two-phase interaction variables (W, F, P) of the uncontrolled combustion process.

The universally independent variable in time-domain is the regular time t. However, for separation of the local and global behavior, the fluid, combustion, and two-phase interaction variables are treated in the form:

$$x(t) \equiv x[t_f(t), t_s(t)] \tag{4}$$

It follows from the above equation that there are two components in $x(t_f, t_s)$: $x'(t_f)$ is only a function of the fast time t_f, governed by the acoustic motion and the other $\tilde{x}(t_s)$ is only a function of the slow time t_s following the mean-flow motion. The two-time scale model is generated as follows:

When observing an event in two different time-scales, we may separate the time-derivative terms $\frac{\partial \rho}{\partial t}$, $\frac{\partial \mathbf{v}_g}{\partial t}$ and $\frac{\partial p}{\partial t}$ in Eqs. (1), (2) and (3) in corresponding two time-scales in the following format, say:

$$\frac{\partial \mathbf{v}_g[\mathbf{r}, t_f(t), t_s(t)]}{dt} = \frac{\partial \mathbf{v}_g}{\partial t_s}\frac{dt_s}{dt} + \frac{\partial \mathbf{v}_g}{\partial t_f}\frac{dt_f}{dt} \equiv \frac{\partial \tilde{\mathbf{v}}_g}{dt_s}\varepsilon_s + \frac{\partial \mathbf{v}'_g}{dt_f}\varepsilon_f \tag{5}$$

Equation (5) implies the fluid variables ρ, $\mathbf{v}_g$ and p can be linearly expanded as, say:

$$\rho(\mathbf{r}, t) = \tilde{\rho}(\mathbf{r}, t_s) + \rho'(\mathbf{r}, t_f) \tag{6}$$

As the slow-time variables are related to system performance, the fast-time variables become related to the internal stability. If proper slow-time dynamics is pursued in operation of the system, based on Eq. (6) and the magnitude orders indicated in the above table, those terms $\mathbf{v}_g \cdot \nabla\rho + \rho\nabla \cdot \mathbf{v}_g$; $\rho \mathbf{v}_g \cdot \nabla \mathbf{v}_g + \nabla p$; $\bar{\gamma} p \nabla \cdot \mathbf{v}_g + \mathbf{v}_g \cdot \nabla p$; (W, F, P); and (W_c, F_c, P_c) in Eqs. (1), (2) and (3) are decomposed into two equations by Taylor series expansion, say, as:

$$\begin{aligned} \rho\nabla \cdot \mathbf{v}_g(\mathbf{r}, t_s, t_f) &= \tilde{\rho}\nabla \cdot \tilde{\mathbf{v}}_g(\mathbf{r}, t_s) + \rho'(\mathbf{r}, t_f)\nabla \cdot \tilde{\mathbf{v}}_g(\mathbf{r}, t_s) \\ &+ \tilde{\rho}(\mathbf{r}, t_s)\nabla \cdot \mathbf{v}'_g(\mathbf{r}, t_f) + \text{higherorder terms} \end{aligned} \tag{7}$$

which follows the following general form

$$\begin{aligned} f[x(t_f, t_s)] = f[\tilde{x}(t_s)] + \frac{\partial f}{\partial x}\Big|_{\tilde{x}(t_s)} x'(t_f) \\ + \text{higher order terms} \cdots\cdots \end{aligned} \tag{8}$$

Finally, the term $\rho\frac{\partial \mathbf{v}_g}{\partial t}$ in Eq. (2) is separated based on Eqs. (5) and (6) as:

$$\rho\frac{\partial \mathbf{v}_g}{\partial t} = (\tilde{\rho} + \rho')\left(\frac{\partial \tilde{\mathbf{v}}}{\partial t_s}\varepsilon_s + \frac{\partial \mathbf{v}'_g}{\partial t_f}\varepsilon_f\right) \tag{9}$$

which is approximated to the first-order accuracy as:

$$\rho\frac{\partial \mathbf{v}_g}{\partial t} \approx \varepsilon_s\tilde{\rho}\frac{\partial \tilde{\mathbf{v}}}{\partial t_s} + \varepsilon_s\rho'\frac{\partial \tilde{\mathbf{v}}_g}{\partial t_s} + \varepsilon_f\tilde{\rho}\frac{\partial \mathbf{v}'_g}{\partial t_f} \tag{10}$$

By using the above first-order approximations (5), (7) and (10), the conservation equations, (1), (2) and (3), are decomposed in two time scales. Collection of those slow-time variables yields

Slow-time Conservation Law:

Mass

$$\begin{aligned} &\varepsilon_s\frac{\partial \tilde{\rho}}{\partial t_s} + \tilde{\mathbf{v}}_g(t_s) \cdot \nabla\tilde{\rho}(t_s) + \tilde{\rho}(t_s)\nabla \cdot \tilde{\mathbf{v}}_g(t_s) \\ &= \tilde{W}(t_s) + \tilde{W}_c(t_s) \end{aligned} \tag{11}$$

Momentum

$$\begin{aligned} &\varepsilon_s\tilde{\rho}(t_s)\frac{\partial \mathbf{v}_g(t_s)}{\partial t_s} + \tilde{\rho}(t_s)\tilde{\mathbf{v}}_g(t_s) \cdot \nabla\tilde{\mathbf{v}}_g(t_s) + \nabla\tilde{p}(t_s) \\ &= \tilde{F}(t_s) + \tilde{F}_c(t_s) \end{aligned} \tag{12}$$

Energy

$$\begin{aligned} &\varepsilon_s\frac{\partial \tilde{p}}{\partial t_s} + \bar{\tilde{\gamma}}\tilde{p}(t_s)\nabla \cdot \tilde{\mathbf{v}}_g(t_s) + \tilde{\mathbf{v}}_g(t_s) \cdot \nabla\tilde{p}(t_s) \\ &= \tilde{P}(t_s) + \tilde{P}_c(t_s) \end{aligned} \tag{13}$$

And collections of fast-time variables yields

Fast-time Conservation Law:

Mass

$$\begin{aligned} &\varepsilon_f\frac{\partial \rho'(t_f)}{\partial t_f} + \tilde{\mathbf{v}}_g(t_s) \cdot \nabla\rho'(t_f) + \mathbf{v}'_g(t_f) \cdot \nabla\tilde{\rho}(t_s) \\ &+ \tilde{\rho}(t_s)\nabla \cdot \mathbf{v}'_g(t_f) + \rho'(t_f)\nabla \cdot \tilde{\mathbf{v}}_g(t_s) \\ &= W'(t_f) + W'_c(t_f) \end{aligned} \tag{14}$$

Momentum

$$\varepsilon_f \tilde{\rho}(t_s)\frac{\partial \mathbf{v}_g'(t_f)}{\partial t_f} + \nabla p'(t_f) = -\tilde{\rho}(t_s)(\tilde{\mathbf{v}}_g(t_s)\cdot\nabla\mathbf{v}_g'(t_f) + \mathbf{v}_g'(t_f)\cdot\nabla\tilde{\mathbf{v}}_g(t_s)) - \rho'(t_f)(\varepsilon_s\frac{\partial\tilde{\mathbf{v}}_g(t_s)}{\partial t_s} + \tilde{\mathbf{v}}_g(t_s)\cdot\nabla\tilde{\mathbf{v}}_g(t_s)) + F'(t_f) + F_c'(t_f) \quad (15)$$

Energy

$$\varepsilon_f\frac{\partial p'(t_f)}{\partial t_f} + \bar{\gamma}\tilde{p}(t_s)\nabla\cdot\mathbf{v}_g'(t_f) = -\bar{\gamma}p'(t_f)\nabla\cdot\tilde{\mathbf{v}}_g(t_s) - \tilde{\mathbf{v}}_g(t_s)\cdot\nabla p'(t_f) - \mathbf{v}_g'(t_f)\cdot\nabla\tilde{p}(t_s) + P'(t_f) + P_c'(t_f) \quad (16)$$

The set of conservation equations (11) to (13) in the slow-time scale governs the mean-flow dynamics, and the set of conservation equations (14) to (16) describes the mean-flow-dependent acoustic dynamics in the fast-time scale.

Subtracting the fast-time derivative of the energy equation (16) from the spatial derivative of the momentum equation (15) yields:

$$\nabla^2 p' - \frac{1}{\bar{a}^2(t_s)}\frac{\partial^2 p'}{\partial {t_f}^2}\varepsilon_f = h + h_c \quad (17)$$

$$h_c = \nabla F_c' - \frac{1}{\bar{a}^2(t_s)}\frac{\partial P_c'}{\partial t_f} \quad (18)$$

where the speed of sound $\bar{a}$ is a local thermodynamic property given by $\bar{a} \equiv \sqrt{\left.\frac{\partial\tilde{p}}{\partial\tilde{\rho}}\right|_s} = \sqrt{\bar{\gamma}\bar{R}\tilde{T}}$ slowly varying in an ideal gas mixture. The function h_c represents the high-frequency control inputs, and h contains the driving and dissipation terms that depend on the spatial and temporal properties of mean-flow temperature and velocity.

The acoustic dynamics is mainly dependent on the mean properties $\tilde{\mathbf{v}}_g$ and $\tilde{T}$ that determines the temporally and spatially compressible properties of the fluid medium in the combustion chamber. Locally and temporally, low $\tilde{T}$ implies reduced speed of sound and consequently the dominant natural frequencies in the combustion medium, and vice versa. The mean-flow velocity $\tilde{\mathbf{v}}_g$ represents the instantaneous and spatial speed of the coordinate frame in which an acoustic mass element travels, providing a driving/dissipated force due to an accelerated/decelerated coordinate frame. Therefore, $\tilde{T}(\mathbf{r},t_s)$ and $\tilde{\mathbf{v}}_g(\mathbf{r},t_s)$ are used as gain-scheduling parameters for control of mean-flow dependent acoustic dynamics.

Since $\tilde{T}(\mathbf{r},t_s)$ and $\tilde{\mathbf{v}}_g(\mathbf{r},t_s)$ are continuously varying with respect to both temporal and spatial variables, measurements with finitely many point sensors may cause loss of relevant information. Furthermore, even if distributed sensors are used to measure the spatial distribution of $\tilde{T}(\mathbf{r},t_s)$ and $\tilde{\mathbf{v}}_g(\mathbf{r},t_s)$, the gain-scheduling control law is likely to be excessively time-consuming and hence unsuitable for on-line computation. To synthesize a control law that is executable in real time on an inexpensive platform, the following approximation is made for spatial representation of the gain-scheduling variables $\tilde{T}(\mathbf{r},t_s)$ and $\tilde{\mathbf{v}}_g(\mathbf{r},t_s)$:

Space-time separation of mean-flow motions

The mean gas velocity $\tilde{\mathbf{v}}_g$ is first separated as the product of the temporal variable t_s and the spatial (vector) variable $\mathbf{r}$ as:

$$\tilde{\mathbf{v}}_g(t_s,\mathbf{r}) \approx \mathbf{v}_t(t_s)\phi_v(\mathbf{r})$$
$$\tilde{T}(t_s,\mathbf{r}) \approx T_t(t_s)\phi_T(\mathbf{r}) \quad (19)$$

where the scalar-valued functions $\phi_v(\mathbf{r})$ and $\phi_T(\mathbf{r})$ are non-negative at each spatial point $\mathbf{r}$. The mass flow rate of gas through a combustor of cross section $A(\mathbf{r})$ is given by:

$$\dot{m}(t) \approx A(\mathbf{r})\tilde{\mathbf{v}}_g(t_s,\mathbf{r})\tilde{\rho}(t_s,\mathbf{r})$$

implying that the mean gas density $\tilde{\rho}$ is inversely proportional to $A(\mathbf{r})\tilde{\mathbf{v}}_g$. Here, the spatial variable $\mathbf{r}$ only includes the longitudinal direction after spatial averaging over the cross-section.

Since the mean pressure $\tilde{p}$ has been assumed to be independent of the spatial variable $\mathbf{r}$ in high-pressure combustors, the ideal gas law dictates that $\tilde{T}$ is inversely proportional to $\tilde{\rho}$. This, in turn, implies that $\tilde{T}$ is directly proportional to $A(\mathbf{r})\tilde{\mathbf{v}}_g$ as:

$$\tilde{T}(t_s,\mathbf{r}) = \frac{\tilde{p}(t)}{\bar{R}\dot{m}(t)}A(\mathbf{r})\mathbf{v}_g(t_s,\mathbf{r}) \quad (20)$$

Using Eq. (19) in Eq. (20) yields:

$$T_t(t_s) \equiv \frac{\tilde{p}(t)}{\bar{R}\dot{m}(t)}\mathbf{v}_t(t_s)$$
$$\phi_t(\mathbf{r}) \equiv A(\mathbf{r})\phi_v(\mathbf{r}) \quad (21)$$

For a combustor of uniform cross-section (i.e., $A(\mathbf{r}) = A$ for all $\mathbf{r}$), the constant term A can be absorbed in the temporal part $T_t(t)$ so that Eq. (21) is modified as:

$$T_t(t_s) = \frac{A\,\tilde{p}(t_s)}{\bar{R}\dot{m}(t_s)}\mathbf{v}_t(t_s)$$
$$\phi_t(\mathbf{r}) \approx \phi_v(\mathbf{r}) \quad (22)$$

Therefore, for uniform cross-section of the combustor, Eq. (19) can be rewritten as:

$$\tilde{\mathbf{v}}_g(t_s,\mathbf{r}) \approx \mathbf{v}_t(t_s)\phi(\mathbf{r})$$
$$\tilde{T}(t_s,\mathbf{r}) \approx T_t(t_s)\phi(\mathbf{r}) \quad (23)$$

where the function $\phi(\mathbf{r})$ is normalized over the total volume V_{comb} of the combustor, i.e.,

$$\frac{1}{V_{comb}}\iiint_V \phi(\mathbf{r})dV = 1 \quad (24)$$

In the sequel, Eq. (23) will be used for modeling combustion dynamics and control systems analysis based on the gain-scheduling variables $\mathbf{v}_t(t_s)$ and $T_t(t_s)$ that are available from the slow-time scale dynamics of the combustion control system. The scheduling variables $\mathbf{v}_t$ and T_t together are referred to as the scheduling vector:

$$\bar{\nu} = \begin{bmatrix}\mathbf{v}_t \\ T_t\end{bmatrix}$$

The speed of sound $\bar{a}$ is expressed as

$$\bar{a} = a_t(t_s)\sqrt{\phi(\mathbf{r})} \quad (25)$$

The pressure perturbation can be modally decomposed as:

$$p'(\mathbf{r},t_f) = \sum_{n=1}^{\infty}\eta_n(t_f)\psi_n(\mathbf{r}) \quad (26)$$

subject to specified boundary conditions along the surface of the chamber. In this coordinate frame, p' has a time-dependent component η_k along the direction of the k^{th} unit vector of an orthonormal basis $\{\psi_n\}_{n=1,2,\cdots}$, which completely spans the space of pressure functions. That is, the set $\{\psi_n\}_{n=1,2,\cdots}$ satisfies the following conditions

- Orthonormality: $\langle \psi_n, \psi_m \rangle \equiv \iiint \psi_n \psi_m dV = \delta_{mn}$ for all integers m and n;
- Completeness: $\langle \varphi, \psi_n \rangle \equiv \iiint \varphi \psi_n dV = 0 \quad \forall n$, then $\varphi = 0$.
- Admissibility: $\psi_n(\mathbf{r})$ satisfies specified boundary conditions $\forall n$

where $\langle \bullet, \bullet \rangle$ defines the inner product.

Modal analysis of acoustic pressure, Eq. (26), is performed as follows.

$$\begin{aligned}
\eta_n &= \iiint \sum_{m=1}^{\infty} \eta_m \psi_m \psi_n dV = \iiint p' \psi_n dV \\
\frac{\partial^2 \eta_n}{\partial t_f^2} &= \iiint \frac{\partial^2 p'}{\partial t_f^2} \psi_n dV \\
&= \iiint \bar{a}^2 \nabla^2 p' dV - \iiint \bar{a}^2 h dV - \iiint \bar{a}^2 h_c dV \\
&= \sum_{m=1}^{\infty} \eta_m \iiint \bar{a}^2(\mathbf{r}, t_s) \nabla^2 \psi_m \psi_n dV + F_n + U_n
\end{aligned} \tag{27}$$

where

$$\begin{aligned}
F_n &= -\iiint \bar{a}^2 h \, dV \\
U_n &= -\iiint \bar{a}^2 h_c \, dV
\end{aligned} \tag{28}$$

In view of Eq. (27) we introduce the following integral relationship:

$$\iiint \bar{a}^2(\mathbf{r}, t_s) \nabla^2 \psi_m \psi_n dV = -\omega_n^2 \delta_{mn} \quad \forall m, n \tag{29}$$

to approximate the mode shapes $\{\psi_n\}_{n=1,2,\cdots}$ and natural frequencies $\{\omega_n\}_{n=1,2,\cdots}$ corresponding to specified boundary conditions. By completeness property of the orthonormal set $\{\psi_n\}_{n=1,2,\cdots}$, Eq. (29) is equivalent to the following algebraic relationship:

$$\bar{a}^2(\mathbf{r}, t_s) \nabla^2 \psi_n(\mathbf{r}) + \omega_n^2(t_s) \psi_n(\mathbf{r}) = 0 \tag{30}$$

A set of ordinary differential equations is derived as an approximation of Eqs. (27) and (28) based on the space-time separation of mean-flow conditions in Eq. (23):

$$\frac{d^2 \eta_n}{dt_f^2} + \omega_n^2(T_t(t_s)) \eta_n = F_n(t_s, t_f) + U_n(t_s, t_f) \tag{31}$$

where

$$F_n \approx -a_t^2 \iiint \phi(\mathbf{r}) h \psi_n(\mathbf{r}) dV \tag{32}$$

$$U_n \approx -a_t^2 \iiint \phi(\mathbf{r}) h_c \psi_n(\mathbf{r}) dV \tag{33}$$

and $\omega_n(t_s) = a_t(t_s) k_n$ (34)

where ω_n is the slowly varying frequency of the n^{th} mode shape, and k_n is the corresponding wave number. Based on the Eqs. (25) and (30), approximated mode shapes are derived as:

$$\phi(\mathbf{r}) \nabla^2 \psi_n + k_n^2 \psi_n = 0 \tag{35}$$

subject to the boundary conditions, where the spatially dependent weighting function $\phi(\mathbf{r})$ puts a smaller weight on the mode shapes of pressure perturbation in the low-temperature region and a larger weight in the high-temperature region.

The fast-time scale control command for secondary fuel injection is superimposed on the slow-time scale primary fuel flow. Control actions arising from the distributed combustion of secondary fuel are modeled by an ensemble of point actuators; the output of each actuator is determined by its position, the local burning characteristics of the fuel, and the time delay from the instant of fuel injection. A detailed derivation of the actuator command U_n in Eq. (33) is presented below [2]:

$$U_n = \frac{-\bar{R} \Delta H_c}{\bar{C}_v} \sum \psi_n(\mathbf{r}_i) u_i(t_f; \bar{\mathrm{v}}) \tag{36}$$

$$u_i = b_i(\bar{\mathrm{v}}) \frac{\partial \dot{m}_{in}[t_f - \tau_i(\bar{\mathrm{v}})]}{\partial t_f} \tag{37}$$

where ΔH_c is the heat of combustion per unit fuel mass and the injection rate of secondary fuel is represented by $\dot{m}_{in}$ with spatial distribution density b_i, the time delay τ_i associated with the ith point actuator.

Finally, the open-loop plant model of the mean-flow dependent acoustic dynamics (in the fast-time scale) becomes

$$\begin{aligned}
&\frac{d^2 \eta_n}{dt_f^2} + \omega_n^2(\tilde{T}(t_s)) \eta_n \\
&+ \sum_{i=1}^{\infty} D_{ni}(\tilde{T}(t_s), \tilde{\mathbf{v}}_g(t_s)) \frac{d\eta_i}{dt_f} + E_{ni}(\tilde{T}(t_s), \tilde{\mathbf{v}}_g(t_s)) \eta_i(t_f) = \\
&- \frac{\bar{R} \Delta H_c}{\bar{C}_v} \sum_k b_k(\tilde{T}(t_s), \tilde{\mathbf{v}}_g(t_s)) \psi_n(\mathbf{r}_k) \frac{\partial \dot{m}_{in}[t_f - \tau_k(\tilde{\mathbf{v}}_g(t_s))]}{\partial t_f}
\end{aligned} \tag{38}$$

The formulation described above is considered as a wide-range model of combustion dynamics and provides a framework for accommodating both the global and local behavior in the two time-scale control systems. For both control and estimation, a state-space realization of the combustion dynamics represents a family of $\bar{\mathrm{v}}$-parameterized models. The models that include uncertainties and effects of mean-flow dependence are presented below:

$$\begin{aligned}
\dot{x}_p &= (A_p(\bar{\mathrm{v}}) + \Delta_p(\bar{\mathrm{v}})) x_p + G_1(\bar{\mathrm{v}}) v + G_2(\bar{\mathrm{v}}) d \\
y &= C x_p + \theta
\end{aligned} \tag{39}$$

where $\bar{\mathrm{v}}$ is the scheduling vector consisting of mean-flow temperature and velocity, d is the plant disturbance and θ is the sensor noise. The state vector is chosen as $x_p = (\varsigma \quad \dot{\varsigma})^T$ with $\dot{\varsigma} = \eta$, and $\eta \equiv [\eta_1, \eta_2, \cdots, \eta_N]^T$. Unsteady heat release Q' and acoustic pressure p' provides *effort* and *flow* information in mechanical systems, where their phase difference determines the dissipated or liberated energy. For the nominal linear model, the system matrix is given as:

$$A_p \equiv \begin{bmatrix} 0 & I \\ -\Omega(T_t) - E(\bar{\nu}) & -D(\bar{\nu}) \end{bmatrix}$$

with $\Omega \equiv diag(\omega_1^2, \omega_2^2, \cdots, \omega_N^2)$ (40)

The input vector $v(t)$ associated with a set of point actuators is related to the mass injection rate of the secondary fuel, $\dot{m}_{in}$, as:

$$v(t) = \begin{bmatrix} b_1(\bar{\nu})\dot{m}_{in}(t - \tau_1(\bar{\nu}) - \delta\tau_1(\bar{\nu})) \\ b_2(\bar{\nu})\dot{m}_{in}(t - \tau_2(\bar{\nu}) - \delta\tau_2(\bar{\nu})) \\ \vdots \\ b_M(\bar{\nu})\dot{m}_{in}(t - \tau_M(\bar{\nu}) - \delta\tau_M(\bar{\nu})) \end{bmatrix} \quad (41)$$

where $\delta\tau_i$ is the modeling error associated with the time delay of the control input. Equation (41) represents the actuator dynamics from the excitation of the point actuator(s) to the actual energy release of control fuel. Since the mean flow is slowly varying compared to the motion of the secondary-fuel injector, the mean-flow-dependent transfer function of actuator dynamics can be approximated as:

$$\boldsymbol{A}(s;\bar{\nu}) = \left[b_1(\bar{\nu})e^{-\tau_1(\bar{\nu})s} \quad b_2(\bar{\nu})e^{-\tau_2(\bar{\nu})s} \quad \cdots \quad b_M(\bar{\nu})e^{-\tau_M(\bar{\nu})s} \right]^T \quad (42)$$

An additive operator $\Delta_p(\bar{\nu})$, that is dependent on the mean-flow conditions, represents the effects of model and parametric uncertainties of the plant. It can be treated as a disturbance to the plant, $w_s = \Delta_p(x_p)$, to realize the energy amplification from input to output through this operator. The global behavior of the operator Δ_p is characterized by the L_2-gain as follows:

$$\left\| \Delta_p(\bar{\nu}) \right\|_\infty < \delta p(\bar{\nu}) \quad (43)$$

A physical interpretation of Eq. (43) is that individual dynamics of the uncertainty operator $\Delta_p(\bar{\nu})$ yields to the following energy amplified relationship from its input x_p to its output w_s as:

$$\int_0^T \left\| w_s \right\|^2 dt < \int_0^T \delta p^2(\bar{\nu}) \left\| x_p \right\|^2 dt \quad \forall T \in [0, \infty) \quad (44)$$

for zero initial conditions.

3. Formulation and Analysis of the Wide-Range Robust Control Law

This section focuses on robust performance issues of the inner-layer within the two-layer wide-range combustion control system as an extension of the narrow-range control concept presented in the previous publication [9]. The acoustic dynamics at the inner layer is parametrically dependent on mean-flow dynamics at the outer-layer. For *robustness*, the inner-layer controller is synthesized such that stability is guaranteed over a wide operating range of persistently varying mean-flow variables and the associated modeling uncertainties. For *performance*, the controller should have the capability for disturbance rejection and meeting the requirements of acoustic energy and control energy under both steady-state and transient conditions. The role of the controller design in this section is to simultaneously satisfy these two objectives for persistently varying mean-flow conditions over a wide range.

3.1 Two-layer Control Structure

In Section 2, the fluid-combustion dynamics have been decomposed into acoustic dynamics in the fast-time scale and mean-flow dynamics in the slow-time scale, in which the parameters of acoustic dynamics are dependent on mean-flow temperature and velocity. In the integrated control strategy, the fluid-combustion dynamics are transformed into a combination of slowly varying trajectory of quasi-steady equilibrium points, defined by mean-flow dynamics, and the associated linear perturbations are defined by the mean-flow-dependent acoustic dynamics in the fast-time scale. While the temporal trajectory of mean-flow variables is tracked for global performance by the slow-time controller, the fast-time controller locally suppresses the acoustic motions with its slowly varying parameters being gain-scheduled by the mean-flow temperature and velocity. The control system of fluid-combustion dynamics is therefore designed to have a two-layer hierarchical structure. The aforementioned mean-flow dynamics represents the open-loop plant in the outer-layer whereas the acoustic dynamics, parametrically dependent on the mean-flow variables, represent the open-loop plant in the inner-layer. The temporal trajectory of mean flow variables is tracked by manipulating the primary-fuel flow in the slow-time scale, while, in the inner-layer, the acoustic dynamics is feedback-controlled by secondary-fuel flow, that is realized as fast modulation of the primary-fuel flow.

Figure 1 and figure 2 show a schematic view of the hierarchical structure of the two-layer control strategy. The inner-layer controller continuously receives gain-scheduled signals from the outer layer to update its parameters that are related to the temporal equilibrium points defined by the mean-flow temperature and velocity, in response to the change of perturbation dynamics at quasi-steady equilibrium points. A slow-time scale mean-flow controller at the outer layer is responsible for global-performance of the combustion chamber. Its design is well known in industry and is not reported in this paper. The inner-layer controller processes the fast-time-scale signals of pressure oscillations and slow-time-scale signals of gain-scheduled variables to modulate the primary-fuel flow. The modulated signal then manipulates the actuator(s) of the combustion chamber to locally suppress perturbations along the temporal trajectory of the mean-flow variables for wide-range control of the combustion dynamics.

3.2 Analysis of the Robust Control Law

To design the robust controller at the inner layer, a family of $\bar{\nu}$-parameterized generalized plants $\boldsymbol{P}(s;\bar{\nu})$ is first constructed following the block diagram in Figure 3. It includes the $\bar{\nu}$-parameterized nominal plant, actuator dynamics, modeling uncertainties and performance requirements for synthesis of a wide-range robust control law. The feedback controller $\boldsymbol{K}(s;\bar{\nu})$ is derived as a function of the gain-scheduling vector $\bar{\nu}$ for controller adaptation under slowly varying operating conditions. Figure 3 shows the internal structure of the $\bar{\nu}$-parameterized generalized plants. The metric of L_2-gain facilitates transformation of the coupled performance-stability robustness analysis problem into a stability robustness problem (Zhou et al., 1996). To incorporate the disturbance rejection capabilities for robust performance, the control objective is related to the metric of L_2 gain, indicating energy amplification from the generic disturbance w to the objective variable z. The generic disturbance w consists of disturbances induced by plant uncertainties w_s, disturbances induced by $\bar{\nu}$-parameterized modeling errors of the time delay function w_τ, weighted plant disturbances w_d, and weighted sensor noise w_θ. The objective variable z consists of stability variables associated with plant uncertainty z_s and time-delay errors z_τ, and performance

variables associated with the acoustic pressure response z_p and the secondary-fuel injection z_u.

The subsystems in the generalized plant family are the nominal plant dynamics specified in the $\bar{\nu}$-parameterized state-space realization, (A_p, G_1, G_2, C), shaping filters associated with the plant disturbances W_d, sensor noise W_θ, performance weighting functions, W_p and W_u, associated with pressure response and secondary-fuel injection, respectively, and the stability weighting function W_τ associated with time-delay errors. Note that the plant uncertainty Δ_p and phase uncertainty Δ_τ induced by time-delay errors are not included because modeling uncertainties are represented as uncertainty-induced disturbances, w_s and w_τ. Two shaping filters W_d and W_θ are incorporated to characterize the main frequency components of the plant disturbances and sensor noise. The performance weighting functions W_p and W_u are specified for the desired frequency responses of acoustic motions and secondary-fuel injection, respectively, providing the trade-off between (high-frequency) transient and (low-frequency) steady-state responses. Those subsystems are derived as analytic functions of the gain-scheduling variable $\bar{\nu}$ to serve as the database of the LPV controller synthesis.

Fast-time modulation of the primary fuel is realized as a secondary-fuel injection. In modeling the secondary-fuel distribution, the possible parametric error of time delay $\delta\tau(\bar{\nu})$ causes $\bar{\nu}$-parameterized phase uncertainty of the closed-loop. The $\bar{\nu}$-parameterized transfer function $e^{-\delta\tau(\bar{\nu})s}$ is represented as one member of the following set:

$$\left\{(1+\Delta_\tau(j\omega;\bar{\nu})W_\tau(j\omega;\bar{\nu})\ \forall\omega\ \forall\bar{\nu} : \left\|\Delta_\tau(j\omega;\bar{\nu})\right\| \le 1\right\} \tag{45}$$

where $\Delta_\tau(j\omega;\bar{\nu})$ accounts for the $\bar{\nu}$-parameterized phase uncertainty and acts as the magnitude scaling for each component of $\bar{\nu}$. The $\bar{\nu}$-parameterized stability weighting function $W_\tau(j\omega;\bar{\nu})$ specifies allowable joint phase-magnitude margins in the closed-loop system and serves as a metric of robustness. Equation (45) is equivalent to:

$$\left|e^{-\delta\tau(\bar{\nu})j\omega} - 1\right| \le \left|W_\tau(j\omega;\bar{\nu})\right|\ \forall\omega\ \ \forall\bar{\nu} \tag{46}$$

where $\delta\tau(\bar{\nu}) \equiv \max_k \left|\tau_k(\bar{\nu})\right|\ \ \forall\bar{\nu}$. For the second source of modeling uncertainty, the $\bar{\nu}$-parameterized plant uncertainty $\Delta_p(s;\bar{\nu})$ acts as an internal feedback to the nominal dynamics. It accounts for modeling inaccuracies of intrinsic coupling between flow dynamics and combustion responses. The bound of $\Delta_p(s;\bar{\nu})$ is specified by its L_2 gain as $\left\|\Delta_p(s,\bar{\nu})\right\|_\infty < \delta_p(\bar{\nu})$. Based on the small gain theorem (Zhou et al., 1996), a sufficient condition of robust stability of the closed-loop system is:

$$\int_0^T \left(\left\|z_s\right\|^2 + \left\|z_\tau\right\|^2\right)dt \le \int_0^T \left(\left\|w_s\right\|^2 + \left\|w_\tau\right\|^2\right)dt\ \ \forall T\in[0,\infty) \tag{47}$$

for the zero-state initial conditions and z_s being equal to $\delta p(\bar{\nu})x_p$.

The inequality in Eq. (47) implies that the robust controller can stabilize all perturbed plants within the $\bar{\nu}$-parameterized uncertainty bounds characterized by $\delta p(\bar{\nu})$ and $\delta\tau(\bar{\nu})$ without specifying any performance requirements that provide trade-off between the control energy and the acoustic energy; transient response and steady-state response; and stability robustness and performance. The performance weights within the system bandwidth are included in the $\bar{\nu}$-parameterized generalized plants for regulation of the secondary-fuel injection and pressure dynamics. Shaping filters are used to penalize the dominant frequency components of plant disturbances and sensor noise for effective rejection. The ability to suppress flow oscillations is quantified by a positive quadratic energy-like function:

$$H = \frac{1}{V}\iiint_V p'(\mathbf{r},t)^2\,dV \tag{48}$$

Orthonormality of the acoustic mode shapes simplifies Eq. (48) as:

$$H = \frac{1}{V}\left\langle\sum\varphi_n\eta_n, \sum\varphi_m\eta_m\right\rangle = \sum\eta_n^2 = \|\eta\|^2 \tag{49}$$

The combustion chamber tends to become free of pressure oscillations if H in Eq. (49) approaches zero.

To achieve small steady-state amplitude and short settling time of pressure oscillations, a new performance variable z_p is introduced as:

$$\hat{z}_p(s) = W_p(s;\bar{\nu})\hat{\eta}(s) \tag{50}$$

where the Laplace Transform of a time-dependent quantity is denoted by "^"; and the weighting function $W_p(s,\bar{\nu})$ is defined as:

$$W_p = \begin{bmatrix} W_{p1} & 0 & \cdots & 0 \\ 0 & W_{p2} & \ddots & \vdots \\ \vdots & \ddots & \ddots & 0 \\ 0 & \cdots & 0 & W_{pN} \end{bmatrix} \tag{51}$$

A procedure for selecting the performance-weighting matrix $W_p(s,\bar{\nu})$ of pressure oscillations is outlined below:

The Bode plot of $W_{pi}(s), i = 1,2,\cdots,N$ resembles that of an integration operator within the bandwidth around each natural frequency $\omega_i(\bar{\nu})$ over the range of the gain-scheduling variable $\bar{\nu}$. The shape of each $W_{pi}(s)$ outside the respective bandwidth is assigned to be flat. The amplitude of each $W_{pi}(s)$ represents the extent of overshoot of the amplitude of its mode shape for trade-off between transient and steady state responses in the sense that a high overshoot usually leads to a short settling time. Thus, the resulting performance variable z_p yields small steady-state amplitude and short settling time of pressure fluctuations. Note that the bandwidth of $W_{pi}(s)$ could be altered by mean-flow-dependent modeling uncertainties. The nominal bandwidth corresponds to the natural frequency of acoustic oscillations. To determine the possible bandwidth range for all perturbed plants, natural frequencies within the uncertainty bound of $\bar{\nu}$ need to be calculated.

The other performance requirement involves secondary-fuel injection. The frequency response of mass flow rate of secondary fuel has limited bandwidth and overshoot amplitude due to the inertial effects of the fuel flow. To this end, a performance weight $W_u(s,\bar{\nu})$ is incorporated into the generalized plant model, and a new performance variable z_u is defined as:

$$\hat{z}_u(s) = W_u(s;\bar{\nu})\hat{u}(s) \tag{52}$$

where $\hat{u}(s)$ and $\hat{z}_u(s)$ are the Laplace transforms of $\dot{m}_{in}(t)$ and $z_u(t)$, respectively. The $\bar{\nu}$-parameterized performance weighting $W_u(s,\bar{\nu})$ is chosen via the following procedure:

The Bode plot of $W_u(s)$ resembles that of a derivative operator within the frequency range of interest. A small z_u implies that the high-frequency component of secondary fuel flow rate $\dot{m}_{in}$ has been filtered out. At each $\overline{\nu}$, the shape of W_u outside the bandwidth is assigned to be flat. The bandwidth range is altered by uncertainties in the (mean-flow-dependent) scheduling vector $\overline{\nu}$.

The nominal performance is specified by the relationship between exogenous inputs, plant disturbance d and sensor noise θ, and performance variables, z_p and z_u. A shaping filer W_d is included in the generalized plant such that the resulting robust controller focuses on rejecting the dominated frequency components of plant disturbance. Therefore, the weighted plant disturbance w_d is used for performance specifications, instead of the disturbance d itself, where

$$\hat{w}_d(s) = W_d(s)\,\hat{d}(s) \tag{53}$$

Similar conditions are introduced in the sensor noise θ as:

$$\hat{w}_\theta(s) = W_\theta(s)\,\hat{\theta}(s) \tag{54}$$

where $\hat{w}_\theta$ is the weighted sensor noise and W_θ is shaping the sensor noise θ.

A linear parameter varying (LPV) robust controller is designed such that the plant disturbance d and sensor noise θ have minimum effects on the acoustic motions and control actions from the energy perspectives. The nominal performance is specified by:

$$\int_0^T \left\| q(\overline{\nu}) z_p(t) \right\|^2 + \left\| z_u(t) \right\|^2 dt \le \int_0^T \left(\left\| w_d(t) \right\|^2 + \left\| w_\theta(t) \right\|^2 \right) dt \quad \forall T \in [0,\infty) \tag{55}$$

where q is a $\overline{\nu}$-parameterized positive scalar, representing the weighting factor of acoustic motion at each $\overline{\nu}$. As q is set larger, then the response of acoustic motions is more emphasized than that of control actions, and vice versa. Furthermore, increasing q implies a better rejection ability of exogenous inputs.

Based on Eq. (47) and Eq. (55), a sufficient condition for robust performance (i.e., a combination of robust stability and nominal performance) of the control system is:

$$\int_0^T \|z\|^2 \, dt \le \int_0^T \|w\|^2 \, dt \quad \forall T \in [0,\infty) \quad \forall w \in L_2[0,T];$$

$$\text{with } z = \begin{bmatrix} z_s \\ q z_p \\ z_u \\ z_\tau \end{bmatrix}; w = \begin{bmatrix} w_s \\ w_d \\ w_\theta \\ w_\tau \end{bmatrix} \tag{56}$$

If Eq. (56) holds, then the controller internally stabilizes the closed-loop for all perturbed plants with desired performance, subject to an uncertainty bound.

Following the internal structure in Fig. 3, the generalized plant family $\boldsymbol{P}(s;\overline{\nu})$ can be expressed, similar to that narrow-range control in the previous publication [9] by state-space realization as:

$$\begin{aligned} \dot{x} &= A(\overline{\nu})x + B_1(\overline{\nu})w + B_2(\overline{\nu})u \\ z &= C_1(\overline{\nu})x + D_{12}(\overline{\nu})u \\ y &= C_2(\overline{\nu})x + D_{21}(\overline{\nu})w \end{aligned} \tag{57}$$

Note that Eq. (56) is conservative because it ignores the structure of the uncertainly robust performance operator $\Delta(s;\overline{\nu})$, which consists of model uncertainties and performance-induced uncertainties. The generalized plant family $\boldsymbol{P}(s;\overline{\nu})$ in Eq. (57) can be compensated to make the requirements of robust performance specified in Eq. (56) less conservative. Figure 4 shows that the generalized plant family is compensated by two $\overline{\nu}$-parameterized compensators, $D^{-1}(s,\overline{\nu})$ and $D(s,\overline{\nu})$. The resulting compensated generalized plant represents the structure Δ without altering the uncertainty size and performance requirements. This is achieved by choosing the D-compensator as:

$$D(s,\overline{\nu})\Delta(s,\overline{\nu}) = \Delta(s,\overline{\nu})D(s,\overline{\nu}) \quad \forall \overline{\nu} \tag{58}$$

This compensation approach, known as the D-K iteration (Packard and Doyle, 1993), can be iterated many times.

4. Synthesis of the Wide-Range Robust Control Law

The inner-layer control law is synthesized using the concept of Linear Parameter Varying (LPV)-L_2-gain methodology that is presented in this section. The objective of the LPV-L_2-gain control law is to reject the effects of chamber disturbances and mean-flow dependent model uncertainties while optimizing the specified performance. The LPV-L_2-gain controller has a H_∞-structure and is derived as a gain-scheduling process accommodating continuous variations of the mean-flow conditions. The major challenge is to synthesize a family of $\overline{\nu}$-parameterized control laws that guarantee robust performance under the continuously varying mean-flow conditions over a wide operating range.

The LPV L_2-gain controller consists of two main components. The first component is a $\overline{\nu}$-parameterized observer that dynamically estimates the states of the $\overline{\nu}$-parameterized generalized plants described by Eq. (57). The estimator structure is not formulated as an exact plant state observer due to the presence of a calibration term $w_{cal}(\overline{\nu})$ that protects the control system from being excessively sensitive to exogenous inputs and modeling uncertainties, entering the observer state equation. The second component is a state-feedback control gain matrix, which determines the control action based on the estimated state $\hat{x}$ as seen in the controller configuration of Figure 5.

The remaining task lies in the determination of the $\overline{\nu}$-parameterized observer matrix $L(\overline{\nu})$, controller matrix $K(\overline{\nu})$, and the calibrated term $w_{cal}(\overline{\nu})$ such that the sufficient condition for robust performance in Eq. (56) holds. Usage of parameter-dependent Lyapunov functions in the controller synthesis leads to differential matrix inequalities as reported by Hong [9]. The results are derived based on the following assumptions,

Assumption#1: The parameter-dependent matrices D_{12} and D_{21} are normalized as:

$$D_{12}(\overline{\nu}) = \begin{bmatrix} 0 \\ I \end{bmatrix}; \; D_{21}(\overline{\nu})\,D_{21}^T(\overline{\nu}) = I; \tag{59}$$

Assumption #2: D_{11} is reduced to zero by loop shifting [10];

Assumption #3: D_{22} is set to zero without loss of generality [10];

Assumption #4: The parameter vector $\overline{\mathbf{v}}(t)$ is a continuous function belonging to a compact subset of $\Re^s$ and the parameter variation rate $\dot{\overline{\mathbf{v}}}(t)$ is bounded as $\left|\dot{\overline{\mathbf{v}}}_i(t)\right| \le \beta_i \quad \forall i \in \{1,2,\cdots,s\}$

Assumption #5: The system matrices of the generalized plant family, $(A, B_1, B_2, C_1, C_2, D_{12}, D_{21})$, are continuous functions of $\overline{\mathbf{v}}$;

Assumption #6: The control matrix $K(\overline{\mathbf{v}})$ and the observer matrix $L(\overline{\mathbf{v}})$ are continuously differentiable functions of $\overline{\mathbf{v}}$;

The main results are summarized below as Theorem 1 below and the detailed proof has been presented by Hong [9].

Theorem 1: All candidate LPV L_2-gain controllers for γ-performance and β-variation are synthesized by solving the following two linearly coupled matrix inequalities for $X(\overline{\mathbf{v}})$ and $Z(\overline{\mathbf{v}})$:

$$\begin{bmatrix} X^{-1}A_X^T + A_X X^{-1} - \sum \pm\beta_i \frac{\partial X^{-1}}{\partial \overline{\mathbf{v}}_i} - B_2 B_2^T & X^{-1}C_1^T(I - D_{12}D_{12}^T) & B_1 \\ (I - D_{12}D_{12}^T)C_1 X^{-1} & -I & 0 \\ B_1^T & 0 & -\gamma^2 I \end{bmatrix} < 0 \quad (60)$$

where $A_X = A - B_2 D_{12}^T C_1$

and

$$\begin{bmatrix} Z^{-1}A_Z + A_Z^T Z^{-1} + \sum \pm\beta_i \frac{\partial Z^{-1}}{\partial \overline{\mathbf{v}}_i} - C_2^T C_2 - C_2^T D_{21} F_1 - F_1^T D_{21}^T C_2 & Z^{-1}B_1 & F_2^T \\ B_1^T Z^{-1} & -I & 0 \\ F_2 & 0 & -\gamma^2 I \end{bmatrix} < 0 \quad (61)$$

where $A_Z = A + B_1 F_1 - B_1 D_{21}^T C_2$

$$F_1 = \frac{1}{\gamma^2} B_1^T X$$

$$F_2 = -(B_2^T X + D_{12}^T C_1)$$

The LPV L_2-gain control law in Figure 5 is derived in terms of the control matrix

$$K(\overline{\mathbf{v}}) = -(B_2^T(\overline{\mathbf{v}})X(\overline{\mathbf{v}}) + D_{12}^T(\overline{\mathbf{v}})C_1(\overline{\mathbf{v}})), \quad (62)$$

the estimation matrix is

$$L(\overline{\mathbf{v}}) = Z(\overline{\mathbf{v}})C_2^T(\overline{\mathbf{v}}), \quad (63)$$

and the calibration term is:

$$w_{\max}(\hat{x}, \overline{\mathbf{v}}) = (B_1(\overline{\mathbf{v}}) - Z(\overline{\mathbf{v}})C_2^T(\overline{\mathbf{v}})D_{21}(\overline{\mathbf{v}}))F_1(\overline{\mathbf{v}})\hat{x} \quad (64)$$

The resulting dynamics of the LPV robust controller becomes

$$\dot{\hat{x}} = [A + B_1F_1 + B_2F_2 - ZC_2^T(C_2 + D_{21}F_1)]\hat{x} + ZC_2^T y$$

$$u = -(B_2^T X + D_{12}^T C_1)\hat{x}$$

where $\hat{x}$ is the estimated state.

The differential matrix inequalities in Theorem 1 are discretized by a finite-element approach as a series of solvable linear matrix inequalities [9]. The commercially available package of Matlab-LMI toolbox that numerically solves these inequalities via a convex optimization procedure has been used for controller synthesis in this paper.

Remark3: Theorem 1 enhances the theory of linear parameter varying (LPV) control in the following two areas:

- The features of the LPV L_2-gain control law in Theorem 1 are similar to those of the existing LTI H_∞ control (Doyle *et al.,* 1989).
- Unlike the LPV control law of Wu et al. (1996), the proposed LPV control is not explicitly dependent on the temporal rates of the scheduling variables. This feature is attractive from the perspectives of real-time implementation because measurements of time derivatives of the scheduling variables may not usually be available.

5. Simulation Results and Discussion

This section presents a series of parametric studies and transient simulations of a generic combustor model to validate the wide-range robust control methodology. The objective is to investigate the relationships among system performance, stability robustness, and plant operation based on the transient response and frequency spectrum of pressure oscillations under different operation scenarios. The relationships among the uncertainty bounds of system dynamics, the response of flow oscillations and control actions, and the allowable variation rates of mean-flow parameters are investigated and quantified.

Table II lists the parameters of the generic combustor that represents typical scenarios encountered in practical combustion chambers. Table III lists the dimensionless quantities that are needed to investigate the four dominant modes of longitudinal acoustic oscillations under H_∞ Control, Gain-scheduled Control, and the LPV-L_2-gain Control. Table IV lists the parameters needed for modeling and simulation.

Two bandwidth-limited performances weighting functions W_p and W_u have been fitted as continuous functions of the scheduling variables: mean-flow temperature $\tilde{T}$ and velocity $\tilde{\mathbf{v}}_g$ at each of the selected modal frequencies $\omega_1, \cdots, \omega_N$. The shaping filters W_d and W_θ are taken as unity as the chamber disturbances and sensor noise are assumed to be white. The system robustness is represented by the bound $\delta p(\overline{\mathbf{v}})$ of plant modeling uncertainties. The system performance is represented by the weighting factor of pressure response $q(\overline{\mathbf{v}})$. The plant operation is characterized by the bounds of absolute values of the normalized rates, $\left|\dot{\rho}_T\right|$ and $\left|\dot{\rho}_v\right|$, respectively, of the scheduling variables $\tilde{T}$ and $\tilde{\mathbf{v}}_g$. Increasing $\left|\dot{\rho}_T\right|$ and $\left|\dot{\rho}_v\right|$ implies that the scheduling variables can be varied faster with guaranteed robust performance. On the other hand, increasing the performance parameters q implies a more stringent requirement of system performance in terms of the transient oscillations of each acoustic mode and the ability to reject chamber acoustic and thermal noise. Extensive simulation experiments have been conducted to realize the trade-off relationship among system robustness, performance and operation of the control system.

The dimensionless bounds of the variation rates $\left|\dot{\rho}_T\right|$ and $\left|\dot{\rho}_v\right|$ jointly define the allowable varying rate of plant operation from the perspectives of performance. Figure 6 shows the trade-off between system performance and plant operation. For the plant uncertainty bound set at $\delta p = 0.03$, the family of curves in Figure 6 serve as a constraint under which the LPV robust controller guarantees system stability and performance in the operating range of dimensionless scheduling variables $\rho_T \in [0.6, 1.4]$ and $\rho_v \in [0.5, 1.5]$. The triple $(\left|\dot{\rho}_T\right|, \left|\dot{\rho}_v\right|, q)$ defines the design point which is evaluated in the modeling

process prior to the controller design. For example, with the maximum variation of the mean-temperature rate $|\dot{\rho}_T|$ being 0.1 and the maximum variation of the mean-velocity variation rate $|\dot{\rho}_v|$ being 0.016, the weighting factor of system performance q should be less than or equal to 0.09 to guarantee robust performance. This is a conservative design and, in the simulation stage, much larger q may be allowed. A larger q leads to a larger risk, since it implies a larger probability that the combustion system may enter into a (potentially) unstable region beyond what is specified by the plant uncertainty model. The insufficient information of uncertainty dynamics, except its size specified by the induced L_2-norm, prevents precise quantification of the region of risk. Figure 6 qualitatively reveals the sensitivity of each design point. Robust performance of the closed-loop system is sensitive to the mean-velocity variation rate $\dot{\rho}_v$ because the L_2-gain control tends to maximize the entropy of the closed-loop system. The effects of mean-velocity rate $\dot{\rho}_v$ on the dissipation or driving force of acoustic dynamics represent the varying condition of the irreversible process in the acoustic field. Since the entropy-oriented scheme is sensitive to the controlled irreversible process, the L_2-gain control system of acoustic dynamics is sensitive to mean-velocity variations. Figure 6 also suggests that the robust performance of the closed-loop is relatively insensitive to the mean-temperature variation rate $\dot{\rho}_T$ because the mean temperature determines the natural frequencies of the acoustic vibration. This phenomenon also leads to the fact that the bandwidth of the open-loop system is almost the same as that of the closed-loop system. In other words, the feedback control does not change the natural frequencies of the system. Therefore, model reduction originally performed in the open-loop plant remains valid after the feedback control is formed. Consequently, for large natural frequencies, the control actions would require fast actuators.

Figure 7 shows that the robust performance of the closed-loop system is not very sensitive to mean temperature variation rate with $|\dot{\rho}_v|$ being set to 0.01. The results indicate that robustness of the closed-loop system becomes sensitive to mean-velocity variation rate only in the region of high performance. Figure 7 can be used to realize a trade-off between robustness δp and performance q. In the low-performance region, the trade-off between robustness and performance is almost linear, i.e., the increment of δp is approximately proportional to the decrement of q.

Two plates in Figure 8 show the temporal trajectories of mean velocity and mean temperature generated from CFD calculation. In the simulation of the closed-loop system for the wide range of mean-flow conditions, the plant uncertainty bound is set to be $\delta p = 0.03$, time delay uncertainty bound $\delta\tau = 3/\omega_0$, plant disturbance intensity $10^{-1}\dfrac{\omega_0^2 \overline{C}_v p_0}{\overline{R}\Delta H_c}$, and sensor noise intensity $10^{-1}\dfrac{\omega_0^2 \overline{C}_v p_0}{\overline{R}\Delta H_c}$. Simulation experiments are conducted under three different controllers:

- Controller #1: Single H_∞ control;
- Controller #2: Gain-scheduled H_∞ control;
- Controller #3: LPV L_2-gain control.

Figure 9 shows the system response using a single H_∞ controller for the entire range of $\rho_T \in [0.6, 1.4]$ and $\rho_v \in [0.5, 1.4]$ where the system response exhibits instability and hence the performance is obviously unacceptable. Note that H_∞ control may be suitable for narrow-range operation as discussed in the previous work (Hong *et. al.*, 1999), but not for wide-range operation here. Figure 10 shows the system performance under the gain-scheduled controller, which is synthesized without considering the variations in the mean-flow variables $\tilde{T}$ and $\tilde{\mathbf{v}}_g$. The results show that the control system is unstable. This establishes the necessity for LPV robust control.

Figures 11, 12, 13 and 14 show the responses of four modes of acoustic oscillations in the combustion chamber under the LPV robust control. The total acoustic oscillations are significantly improved since the controller exhibits the ability to reject exogenous inputs on the first two modes without degrading the responses of high-frequency modes. This suggests that model reduction has not caused any significant loss of robustness under the LPV control for wide-range operation. Therefore, usage of LPV robust control may not require a meticulous consideration of the high-frequency excitation provided that the scheduling variables are appropriately rate-bounded. It is also shown that the closed-loop system is asymptotically stable in the absence of exogenous inputs.

The embedded observer located in the LPV robust controller is capable of estimating the internal states of acoustic dynamics under a wide range of continuously varying mean-flow condition as seen in Figures 11, 12, 13 and 14. The embedded observer provides an estimation of acoustic vibration of each mode. The transient and steady-state errors, due to modeling uncertainties and exogenous inputs, are shown to be small. This implies that the calibration terms in the embedded observer are able to keep the system away from the high-risk region, and yet they are small enough not to significantly change the estimated states. In the absence of modeling uncertainties, the performance of the observer embedded in L_2-gain controller approaches that of the minimum variance state estimator.

Figure 15 shows the secondary-fuel injection in the LPV robust control system. The fast-time modulation does not cross 4 % of primary fuel flow rate, while the amplitude of acoustic pressure oscillations exceeds 10% of the mean pressure. Figure 16 shows the frequency spectrum of the normalized pressure perturbations before and after the controller is brought in. The responses exhibit two frequency-scaled components corresponding to two time-scaled motions.

6. Summary and Conclusions

To synthesize a robust control law for wide-range operations, a two-time-scale model of combustion dynamics has been formulated by decomposition of the conservation laws and thermodynamic state relations based on the slowly varying mean-flow and fast perturbed conditions of the process variables. The fast-time scale acoustic-flame dynamics are parametrically dependent on the mean-flow temperature and velocity. Control actions on the fast-time scale are provided by secondary fuel injection that is realized as fast modulation of the primary fuel flow. The structure of control system follows a two-layered hierarchy. In the outer-layer, mean-flow dynamics of the combustion process is controlled in the slow-time scale by manipulating the primary-fuel flow, while the fast-time acoustic controller in the inner-layer is parametrically gain-scheduled by the mean-flow temperature and velocity from the outer-layer.

In the fast-time scale inner-layer, a robust control law is formulated based on the concept of linear parameter varying (LPV) L_2-gain in the setting of differential game theory. The LPV L_2-gain control law has an embedded observer that dynamically estimates the plant states. Time derivatives of the gain-scheduling variables need not be computed or estimated to realize the interactions between inner-layer and outer-layer segments of the control system.

For both narrow-range and wide-range conditions of the mean-flow variables, the robust control law is designed in terms of robustness, performance and parameter variation rate. Procedures for selection of mean-low-dependent and frequency-dependent weighting functions have been proposed in this paper. Physics of the thermo-acoustic phenomena have a significant bearing upon the selection of these performance weights and very little iterations are needed to arrive at the final design of the robust control law. In addition, a numerical tool for synthesis of the LPV robust control law is formulated based on the concept of finite-element analysis. Parametric studies and simulation experiments have been performed to evaluate the robust control system in terms of trade-off between: (i) fuel injection and pressure oscillations; (ii) transient response and steady response; and (iii) stability robustness and performance.

The results generated in this paper potentially lead to a design methodology for wide-range robust control of pressure oscillations in a generic combustor. The findings of this paper could be applied to a multitude of other combustion processes. Although the simulated results clearly indicate efficacy of the robust controller design methodology, several issues concerning implementation of robust control laws need to be addressed before applications to operating combustors.

Acknowledgements

The research work reported in this paper has been supported in part by the Office of Naval Research under Grant No. N00014-96-1-0405.

References

1. Yang, V., Santavicca, D. A., and Ray, A., *Proceedings of Twelfth ONR Propulsion Meeting*, 1999, p. 61-66.
2. Fung, Y. T., Yang, V., and Sinha, A., *Comb. Sci. Technol.*, 78:217-245 (1991).
3. Yang, V., Sinha, A., and Fung, Y. T., *J. Propulsion and Power*, 8:66-73 (1992).
4. Fung, Y. T., and Yang, V., *J. Propulsion and Power*, 8:66-73.
5. Koshigoe, S., Komatsuzaki, T., and Yang, V., *J. Propulsion and Power*, 15:383-389 (1999).
6. Hong, B. S., Yang, V., and Ray A., C*omb. Flame*, 120:91-106 (2000).
7. Packard, A., *Systems and Control Letters*, 22:79-92 (1994).
8. Wu, F., Yang, X. H., Packard A., and Becker, G., *International Journal of Robust and Nonlinear Control*, 6:983-998 (1996).
9. Hong, B. S. *Robust Control of Combustion Instabilities* Ph.D. Dissertation, The Pennsylvania State University, 1999.
10. Zhou, K., Doyle, J. C., and Glover, K., *Robust and Optimal Control*, Prentice-Hall, New Jersey, 1996

Table II. Parameters of the Generic Combustion Chamber

Time average sound speed a_0	795.8 m/s
Time average mean temperature T_0	1415 K
Time average mean pressure p_0	0.5 Mpa
Combustor length L	1.0 m
Combustor diameter d_c	0.6 m
Specific heat ratio $\overline{\gamma}$	1.2
Gas constant $\overline{R}$	373 J/(kg.K)
Constant volume specific heat $\overline{C}_v$	1500 J/(kg.K)
(MMH) heat of combustion (ΔH_c)	5×10^6 J/kg
Average fundamental frequency $\omega_0 \equiv \pi a_0 / L$	1000 rad/s
Average mean velocity $\mathbf{v}_0$	300 m/s
Average mixed density $\overline{\rho}$	0.9473 kg/m^3

Table III Dimensionless Quantities

Dimensionless time t'	$\omega_0 t$
Dimensionless frequency ω'	ω / ω_0
Dimensionless injected rate of control-fuel u'	$\dfrac{-\overline{R}\Delta H_c}{\omega_0^2 \overline{C}_v p_0} u$
Dimensionless damping ratio D'_{ni}	D_{ni} / ω_0
Dimensionless frequency shifting E'_{ni}	E_{ni} / ω_0^2
Dimensionless gain-scheduling mean velocity ρ_v	$\mathbf{v}_t / \mathbf{v}_0$
Dimensionless gain-scheduling mean temperature ρ_T	T_t / T_0
Dimensionless ρ_v variation rate $\dot{\rho}_v$	$d\rho_v / dt'$
Dimensionless ρ_T variation rate $\dot{\rho}_T$	$d\rho_T / dt'$

Table IV Parameters Used in Simulation and Modeling

Maximum time delay error	$\delta\tau = 3/\omega_0$
Plant uncertainty bound	$\delta p = 0.03$
Weighting factor	$q = 0.1$
White plant disturbance intensity	$10^{-1}\ \dfrac{\omega_0^2 \overline{C}_v p_0}{\overline{R}\Delta H_c}$
White sensor noise intensity	$10^{-1}\ \dfrac{\omega_0^2 \overline{C}_v p_0}{\overline{R}\Delta H_c}$
Initial conditions	an impulse $0.01\ p_0$ /sec.

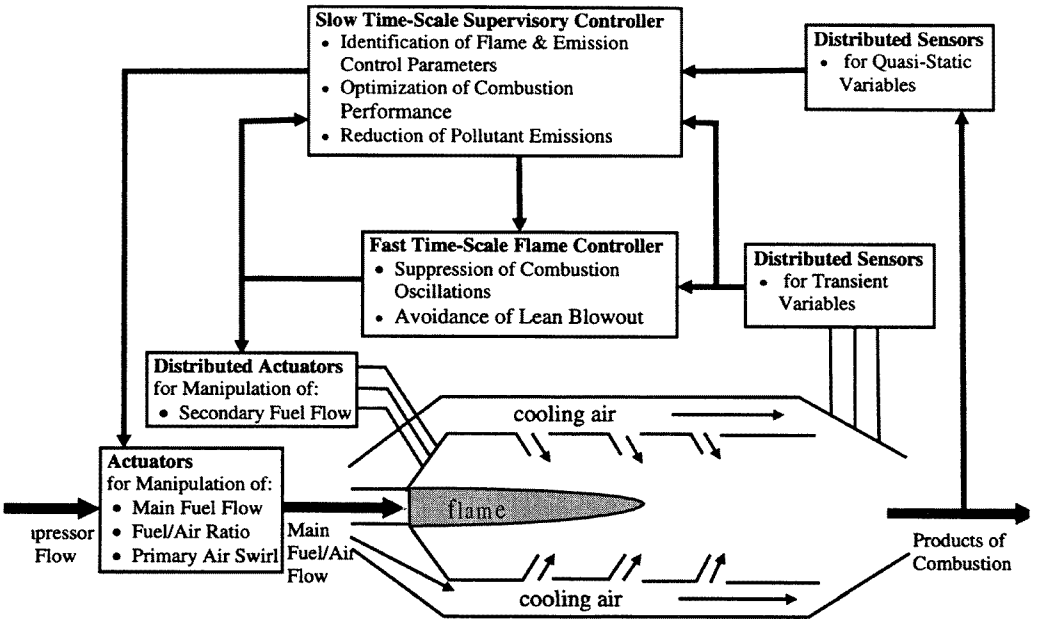

Figure 1 Two-layer Control System for Modulating Combustion Dynamics

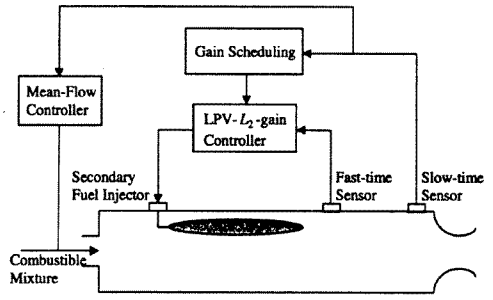

Figure 2 Two-Layer Robust Control System for Combustion Dynamics

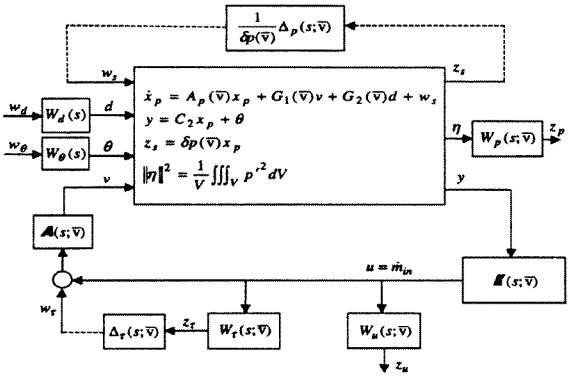

Figure 3 Mean-flow Parameterized, Generalized Plant of Combustion Dynamics

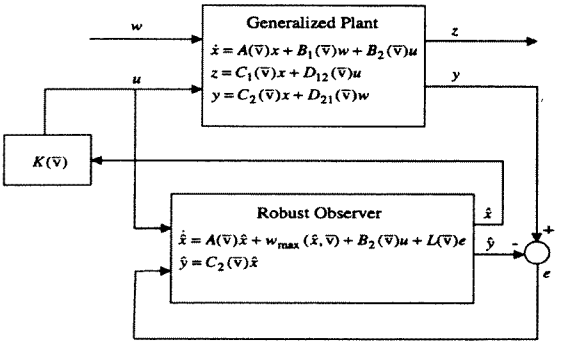

Figure 5 Synthesis of LPV Robust Control System

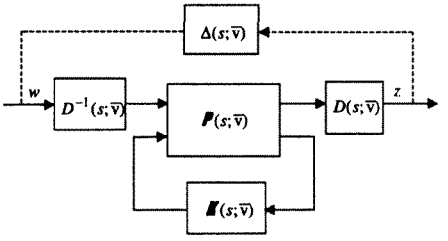

Figure 4 Compensated Generalized Plant of Combustion Dynamics

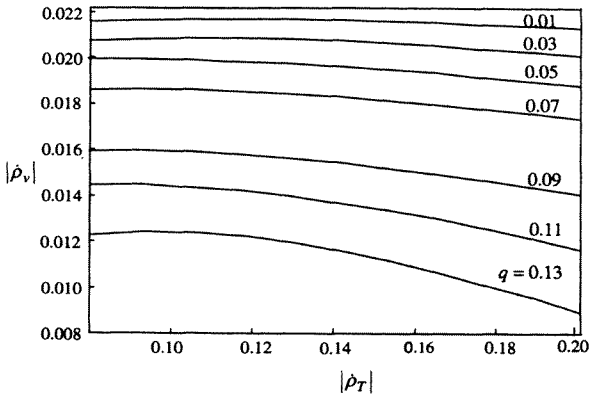

Figure 6 Trade-off between Performance and Plant Operation

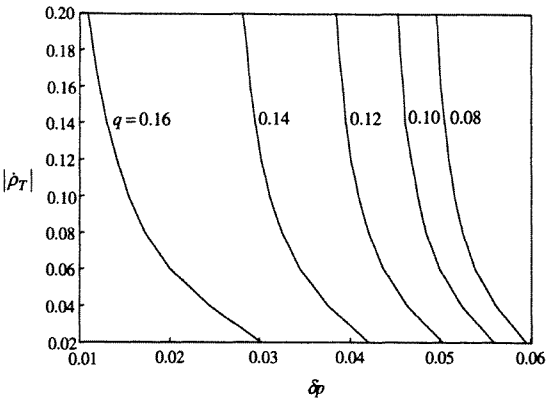

Figure 7 Trade-off between Robustness and Performance

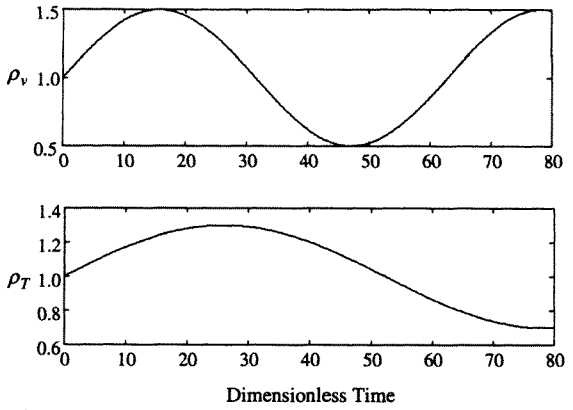

Figure 8 Time History of Mean Velocity and Temperature

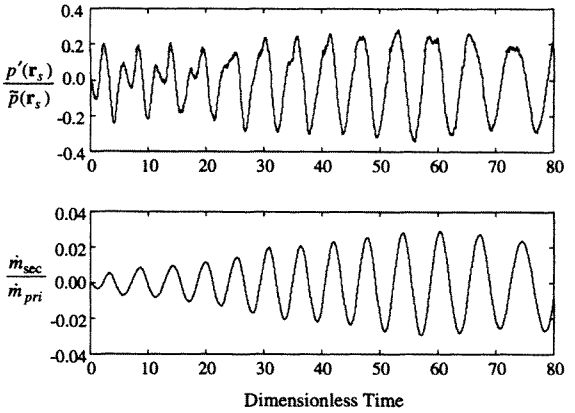

Figure 9 System Response under H_∞ Control

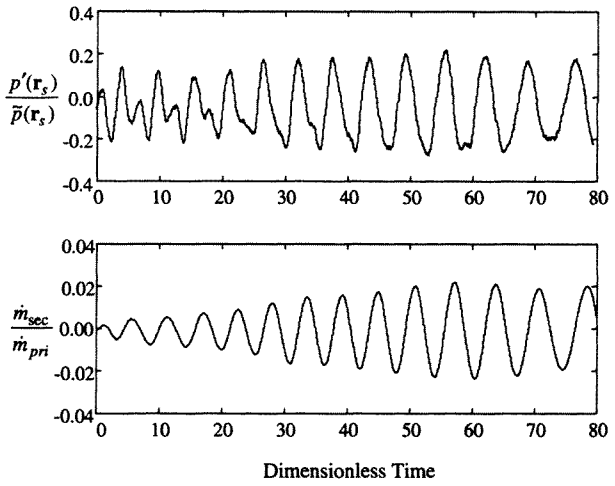

Figure 10 System Response under Gain-Scheduled Control

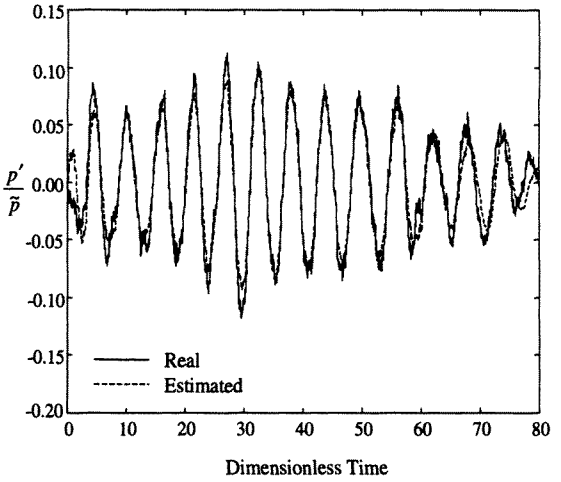

Figure 11 Time History of First-Mode of Pressure Oscillation under LPV-L_2- Gain Control

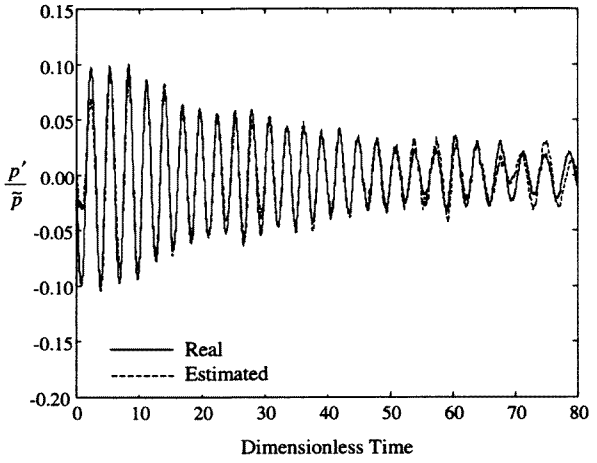

Figure 12 Time History of Second-Mode of Pressure Oscillation under LPV-L_2 - Gain Control

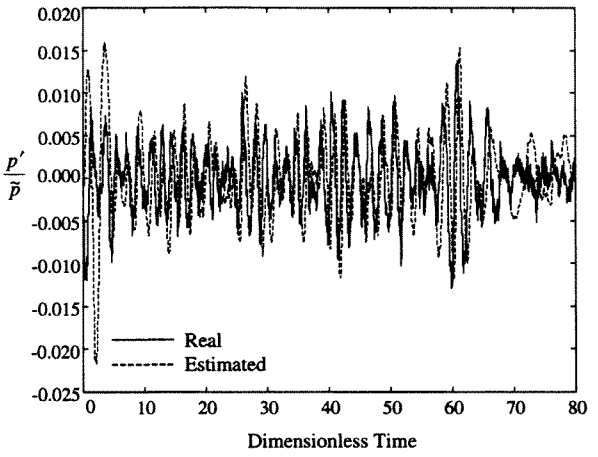

Figure 13 Time History of Third-Mode of Pressure Oscillation under LPV-L_2 - Gain Control

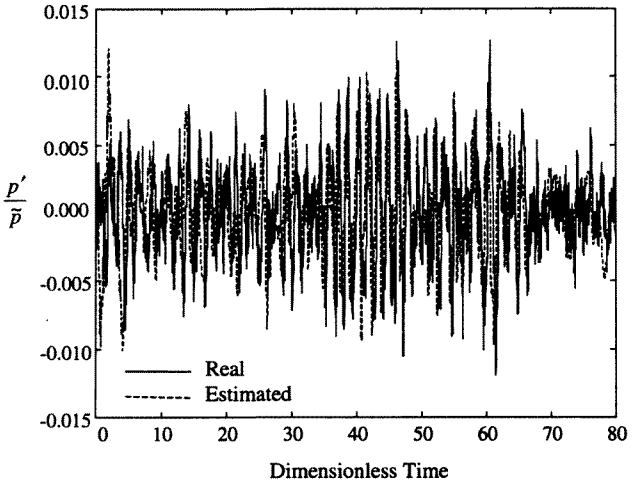

Figure 14 Time History of Fourth-Mode of Pressure Oscillation under LPV-L_2 - Gain Control

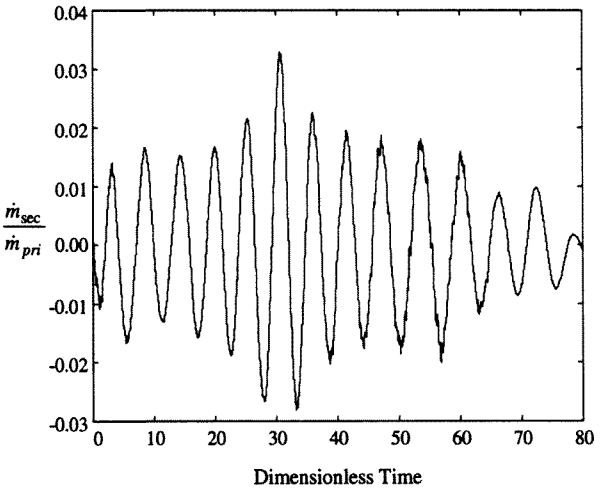

Figure 15 Secondary Fuel Injection Rate under LPV L_2-Gain Control

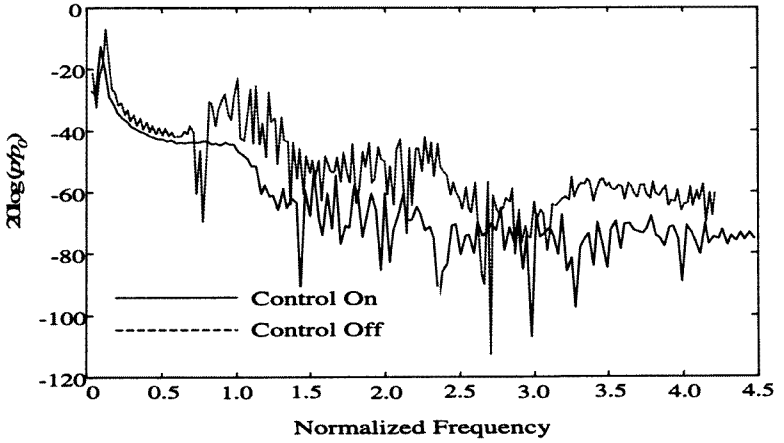

Figure 16 Frequency Spectrum of Pressure with and without LPV L_2-gain Control